Supersonic Base Flow by Using High Order Schemes

Edward Jae-Ryul Shin, Su-Hee Won**, Doek-Rae Cho* and Jeong-Yeol Choi**
**Pusan National University, Busan, South Korea, 609-735*
***Seoul National University, Seoul, South Korea, 151-741*
aerochoi@pusan.ac.kr

Keywords: Roe, AUSMDV, WENO, MUSCL, Limiter

Abstract

We performed numerical analysis of base drag phenomenon, when a projectile with backward step flies into atmosphere at supersonic speed. We compared with other researchers. From our previous studies that were 2-dimensional simulation[1)], we found out from sophisticated simulations that need dense mesh points to compare base pressure and velocity profile after from base with experimental data. Therefore, we focus on high order spatial discreretization over 3rd order with TVD such as MUSCL TVD 3rd, 5th[2)], and WENO 5th order[3)], and Limiters such as minmod, Triad. Moreover, we enforce to flux averaging schemes such as Roe[4)], RoeM, HLLE, AUSMDV[5)].

In present, one dimensional result of Euler tests, there are Sod, Lax, Shu-Osher and interacting blast wave problems. AUSMDV as a flux averaging scheme with MUSCL TVD 5th order as spatial resolution is good agreement with exact solutions than other combinations. We are carrying out the same approaches into 3-dimensional base flow only candidate flux schemes that are Roe, AUSMDV. Additionally, turbulence models are used in 3-dimensional flow, one is Menter's SST DES model[6)] and another is Sparlat-Allmaras DES/DDES model[7)] in Navier-Stokes equations.

Theoretical Fundamental

Governing Equations

Fluid flow is governed by the Navier-Stokrs equations. The governing equations can be summarized as a following conservation form, the continuity, momentum, and energy equation.

$$\frac{\partial r}{\partial t}+\frac{\partial ru_i}{\partial x_j}=0 \tag{1}$$

$$\frac{\partial ru_i}{\partial t}+\frac{\partial}{\partial x_j}(ru_iu_j+pd_{ij})=\frac{\partial t_{ij}}{\partial x_j} \tag{2}$$

$$\frac{\partial re_t}{\partial t}+\frac{\partial}{\partial x_i}(re_t+p)u_i=\frac{\partial u_j s_{ij}}{\partial x_j}-\frac{\partial q_i}{\partial x_i} \tag{3}$$

$$p=rRT \tag{4}$$

$$t_{ij}=m\left(\frac{\partial u_i}{\partial x_j}+\frac{\partial u_j}{\partial x_i}-\frac{2}{3}\frac{\partial u_k}{\partial x_k}d_{ij}\right) \tag{5}$$

$$q_i=k\frac{\partial T}{\partial x_i} \tag{6}$$

Where r, u_i, e_t, s_{ij} and q_i are density, the velocity components, total energy per unit mass, viscous stress tensors and heat flux, respectively. d_{ij} is kronecker symbol. The system of equations is followed by a perfect gas. For the perfect gas of the equation of state is eq. (4). R is the gas constant.

Menter's SST DES Formulation

The $K-w$ model of Wilcox[8)] with a high Reynolds number $K-e$ model is well behaved in the near-wall region, where needs no damping function. However, the model is strongly sensitive to the free stream value of w. This sensitivity seems to be a factor mainly for free shear flows, and does not seem to adversely affect boundary layer flows. On the other hand, the $K-e$ equations are relatively insensitive to free stream values, but behave poorly in the near wall region.

Menter proposed a combined $K-e$ / $K-w$ model which uses the best features of each model. The model uses a parameter F_1 to switch from $K-w$ to $K-e$ in the wake region to prevent the model from being sensitive to free stream conditions.

$$\frac{\partial rK}{\partial t}+\frac{\partial ru_jK}{\partial x_j}=P_K-b^*rKw+\frac{\partial}{\partial x_j}\left[(m+s_Km_t)\frac{\partial K}{\partial x_j}\right] \tag{7}$$

$$\frac{\partial rw}{\partial t}+\frac{\partial ru_jw}{\partial x_j}=a\frac{w}{K}P_K-brw^2+\frac{\partial}{\partial x_j}\left[(m+s_wm_t)\frac{\partial w}{\partial x_j}\right]+2(1-F_1)rs_{w2}\frac{1}{w}\frac{\partial K}{\partial x_j}\frac{\partial w}{\partial x_j} \tag{8}$$

The terms on the right-hand side of eq. (7)~(8) represent eddy-viscosity production, dissipation and conservative diffusion, respectively. Furthermore, the last term in the w-equation describes the cross diffusion.

The turbulent eddy viscosity is obtained from

$$m_t=\frac{a_1rK}{\max(a_1w,\Omega F_2)} \tag{9}$$

The eddy-viscosity production of turbulence is given by

$$P_K=t_{ij}\frac{\partial u_i}{\partial x_j}, \tag{10}$$

$$t_{ij}=m_t\left(\frac{\partial u_i}{\partial x_j}+\frac{\partial u_j}{\partial x_i}-\frac{2}{3}d_{ij}\frac{\partial u_k}{\partial x_k}\right)-\frac{2}{3}rKd_{ij}. \tag{11}$$

The function F_1 in eq. (8), which blends the model coefficients of the $K-w$ model in boundary layers with the transformed $K-e$ model in free-shear layers and free stream zones, is defined as

$$F_1=\tanh\left[\left[\min\left[\max\left(\frac{\sqrt{K}}{b^*wd},\frac{500m}{rwd^2}\right),\frac{4rs_{w2}K}{CD_{Kw}d^2}\right]\right]^4\right] \tag{12}$$

Where d stands for the distance to the nearest wall and CD_{Kw} is the positive part of the cross-diffusion term.

$$CD_{Kw} = \max\left(2r s_{w2}\frac{1}{w}\frac{\partial K}{\partial X_j}\frac{\partial w}{\partial X_j}, 10^{-20}\right) \quad (13)$$

The auxiliary function F_2 in eq. (9) is given by

$$F_2 = \tanh\left[\left[\max\left(\frac{2\sqrt{K}}{b^* w d}, \frac{500m}{r w d^2}\right)\right]^2\right] \quad (14)$$

The model constants are

$a_1 = 0.31$, $b^* = 0.09$, $k = 0.41$

Finally, the coefficients of the SST turbulence model b, a, s_K and s_w are obtained by blending the coefficients of the $K-w$ model, denoted as f_1, with those of transformed $K-e$ model denoted as f_2. The corresponding relation reads

$$f = F_1 f_1 + (1-F_1) f_2 \quad (15)$$

The coefficients of the inner model $K-w$ are given by

f_1; $s_{K1} = 0.85$, $s_{w1} = 0.5$, $b_1 = 0.075$

$$a_1 = \frac{b_1}{b^*} - s_{w1}k^2/\sqrt{b^*} = 0.533$$

The coefficients of the outer model $K-e$ are given by

f_2; $s_{K2} = 1.0$, $s_{w2} = 0.856$, $b_2 = 0.0828$

$$a_2 = \frac{b_2}{b^*} - s_{w2}k^2/\sqrt{b^*} = 0.440$$

Strelets[6] introduced a DES model based on Menter's SST model. In the SST model, the turbulent length scale of the model in terms of K and w reads

$$l_{K-w} = K^{1/2}/(b^* w). \quad (16)$$

This length scale should be replaced in DES modification length scale.

$$\tilde{l} = \min(l_{K-w}, C_{DES}\Delta), \quad \Delta = \max(\Delta x, \Delta y, \Delta z) \quad (17)$$

The only term of the SST model is the dissipative term of the K-transport equation.

$$D^K_{RANS} = r b^* K w = r K^{3/2}/l_{K-w} \quad (18)$$

The modification of DES dissipation term of the K-transport equation is

$$D^K_{DES} = r K^{3/2}/\tilde{l} \quad (19)$$

Menter's SST model is based on a blending of $K-e$ and $K-w$, Strelets calibrated the model by running both the $K-e$ and $K-w$ DES models on isotropic turbulence.

This lead to $C^{K-e}_{DES} = 0.61$ and $C^{K-w}_{DES} = 0.78$. The traditional blending function was used to blend between the two constants,

$$C_{DES} = F_1 C^{K-w}_{DES} + (1-F_1) C^{K-e}_{DES}. \quad (20)$$

The recommended constants were used in the current study.

Spalart-Allmaras DES / DDES Formulation

The Spalart-Allmaras one-equation model solves a single partial differential equation for a variable $\tilde{n}$ which is related to the turbulent viscosity. The model includes a wall destruction term that reduces the turbulent viscosity in the log layer and laminar sublayer, and trip terms that provide a smooth transition from laminar to turbulent.

The Spalart-Allmaras turbulence model can be written in tensor notation as follows.

$$\frac{\partial r\tilde{n}}{\partial t} + \frac{\partial}{\partial X_j}(r\tilde{n}v_j) = C_{b1}\tilde{S}r\tilde{n} + \frac{1}{s}\left\{\frac{\partial}{\partial X_j}\left[(m+r\tilde{n})\frac{\partial\tilde{n}}{\partial X_j}\right] + C_{b2}r\frac{\partial\tilde{n}}{\partial X_j}\frac{\partial\tilde{n}}{\partial X_j}\right\} - rC_{w1}f_w\left(\frac{\tilde{n}}{d}\right)^2 \quad (21)$$

The terms on right-hand side represent eddy-viscosity production, conservative diffusion, non-conservative diffusion and near-wall turbulent destruction.

The turbulent eddy viscosity is obtained from

$$m_t = f_{v1} r\tilde{n} \quad (22)$$

The production term is evaluated with the following formulae

$$f_{v1} = \frac{c^3}{c^3 + C^3_{v1}}, \quad \tilde{S} = S + \frac{\tilde{n}}{k^2 d^2} f_{v2}, \quad (23)$$

$$f_{v2} = 1 - \frac{c}{1 + c f_{v1}}, \quad c = \frac{\tilde{n}}{n}. \quad (24)$$

The term controlling the destruction of the eddy viscosity read

$$f_w = g\left(\frac{1+C^6_{w3}}{g^6 + C^6_{w3}}\right)^{1/6}, \quad (25)$$

$$g = r + C_{w2}(r^2 - r), \quad r = \frac{\tilde{n}}{\tilde{S}k^2 d^2} \quad (26)$$

The various constants are defined as

$C_{b1} = 0.1355$, $C_{b2} = 0.622$, $C_{v1} = 7.1$, $C_{v2} = 5$

$s = 2/3$, $k = 0.4187$, $C_{w1} = C_{b1}/k^2 + (1+C_{b2})/s$

$C_{w2} = 0.3$, $C_{w3} = 2$

The standard Spalart-Allmaras model uses the distance to the closest wall as the definition for the length scale d, which plays a major role in determining the level of production and destruction of turbulent viscosity. The DES model, as proposed by Shur *et al.*[9] replaces d everywhere with a new length scale $\tilde{d}$, defined as

$$\tilde{d} = \min(d, C_{DES}\Delta), \quad \Delta = \max(\Delta x, \Delta y, \Delta z) \quad (27)$$

Where the grid spacing, Δ, is based on the largest grid space in the x, y or z directions forming the computational cell. The empirical constant C_{DES} has a value of 0.65.

For Delayed Detached Eddy Simulation (DDES)[7], the parameter r is slightly modified relative to the S-A definition, in order to apply to any eddy-viscosity model, and be slightly more robust in irrotational regions.

$$r_d \equiv \frac{n_t + n}{\sqrt{U_{i,j}U_{i,j}}k^2 d^2} \quad (28)$$

Similar to r in the S-A model, this parameter equal 1 in a logarithmic layer, and falls to 0 gradually towards the edge of the boundary layer.

The quantity r_d is used in the function.

$$f_d \equiv 1 - \tanh\left(\left[8r_d\right]^3\right) \quad (29)$$

Which is designed to be 1 in the LES region, where r_d 1, and 0 elsewhere.

The application of the above procedures to S-A based DES, proceeds by re-defining the DES length scale $\tilde{d}$:

$$\tilde{d} \equiv d - f_d \max(0, d - C_{DES}\Delta) \quad (30)$$

Setting f_d to 0 yields RANS ($\tilde{d} = d$), while setting it to 1 gives $\tilde{d} = \min(d, C_{DES}\Delta)$.

Computational Algorithm

Flux Splitting Methods

Flux quantities are computed using Roe[4] flux difference splitting. The flux across each cell face $i+1/2$ is computed using Roe numerical flux formula:

$$\mathbf{E}_{i+1/2} = \tfrac{1}{2}\left[\mathbf{E}(\mathbf{Q}^{\mathrm{L}}) + \mathbf{E}(\mathbf{Q}^{\mathrm{R}}) - |\mathbf{A}|(\mathbf{Q}^{\mathrm{R}} - \mathbf{Q}^{\mathrm{L}})\right]_{i+1/2} \quad (31)$$

Here $\mathbf{Q}^{\mathrm{L}}$ and $\mathbf{Q}^{\mathrm{R}}$ are the state variables to the left and right of the interface $i+1/2$. The matrix $\mathbf{A}$ is computed from evaluating

$$\mathbf{A} \equiv \frac{\partial \mathbf{E}}{\partial \mathbf{Q}} \quad (32)$$

with Roe-averaged quantities such as:

$$r = \sqrt{r_{\mathrm{L}} r_{\mathrm{R}}} \quad (33)$$

$$u_i = \left(u_{i,\mathrm{L}} + u_{i,\mathrm{R}}\sqrt{r_{\mathrm{R}} r_{\mathrm{L}}}\right) \Big/ \left(1 + \sqrt{r_{\mathrm{R}} / r_{\mathrm{L}}}\right) \quad (34)$$

$$h = \left(h_{\mathrm{L}} + h_{\mathrm{R}}\sqrt{r_{\mathrm{R}} r_{\mathrm{L}}}\right) \Big/ \left(1 + \sqrt{r_{\mathrm{R}} / r_{\mathrm{L}}}\right) \quad (35)$$

$$a^2 = (g-1)\left(h - \tfrac{1}{2}u_i^2\right) \quad (36)$$

So that

$$\mathbf{E}(\mathbf{Q}^{\mathrm{R}}) - \mathbf{E}(\mathbf{Q}^{\mathrm{L}}) = |\mathbf{A}|(\mathbf{Q}^{\mathrm{R}} - \mathbf{Q}^{\mathrm{L}}) \quad (37)$$

is satisfied exactly.

AUSMDV was constructed with an aim at removal numerical dissipation of Van Leer-type vector splitting on a contact discontinuity[5]. The flux across each cell face $i+1/2$ is computed using AUSMDV numerical flux formula:

$$\mathbf{E}_{i+1/2} = \frac{1}{2}\begin{cases}(\rho u)_{i+1/2}(\mathbf{Q}^{\mathrm{L}} + \mathbf{Q}^{\mathrm{R}}) \\ |(ru)_{i+1/2}|(\mathbf{Q}^{\mathrm{R}} - \mathbf{Q}^{\mathrm{L}})\end{cases} + \mathbf{p}_{i+1/2} \quad (38)$$

The AUSMV scheme in which only the $(ru^2)_{i+1/2}$ in the normal momentum uses FVS:

$$(ru^2)_{\mathrm{AUSMV}} = u_{\mathrm{L}}^{+}(ru)_{\mathrm{L}} + u_{\mathrm{R}}^{-}(ru)_{\mathrm{R}} \quad (39)$$

The AUSMD scheme has in the normal momentum:

$$(ru^2)_{\mathrm{AUSMD}} = \frac{1}{2}\begin{cases}(\rho u)_{i+1/2}(u_{\mathrm{L}} + u_{\mathrm{R}}) \\ |(ru)_{i+1/2}|(u_{\mathrm{R}} - u_{\mathrm{L}})\end{cases} \quad (40)$$

This scheme is a mixture of AUSMV and AUSMD, it is modified the normal momentum flux $(ru^2)_{i+1/2}$ as follows:

$$(ru^2)_{\mathrm{i+1/2\ AUSMDV}} = \frac{1}{2}(1+s)(ru^2)_{\mathrm{AUSMV}} + \frac{1}{2}(1-s)(ru^2)_{\mathrm{AUSMD}} \quad (41)$$

Where, s is a switching function of the pressure gradient:

$$s = \min\left(1, K\frac{|p_{\mathrm{R}} - p_{\mathrm{L}}|}{\min(p_{\mathrm{L}}, p_{\mathrm{R}})}\right), \ 0 \le s \le \frac{1}{2}, \ K = 10 \quad (42)$$

The high order accuracy of $\mathbf{E}_{i+1/2}$ is determined by achieving the high order accuracy of the left and right conservative variables $\mathbf{Q}^{\mathrm{L}}$ and $\mathbf{Q}^{\mathrm{R}}$.

Reconstruction Methods

A third-order MUSCL scheme, a fifth-order MUSCL scheme and a fifth-order WENO method are investigated. MUSCL approach is based on additional dependence on adjacent points in order to bring higher order accuracy in space. In variable interpolation approach, extrapolated values for left and right side are calculated as below:

$$\mathbf{Q}_{i+1/2}^{\mathrm{L}} = u_i + 0.5 f(r_{\mathrm{L}})\Delta u_{i-1/2}, \quad (43)$$

$$\mathbf{Q}_{i+1/2}^{\mathrm{R}} = u_{i+1} - 0.5 f(r_{\mathrm{R}})\Delta u_{i+3/2}. \quad (44)$$

where, u is conservative variables vector and i is cell index.

$$\Delta u_{i-1/2} = u_i - u_{i-1}, \ r_{\mathrm{L},i} = \frac{\Delta u_{i+1/2}}{\Delta u_{i-1/2}}, \ r_{\mathrm{R},i} = \frac{\Delta u_{i+1/2}}{\Delta u_{i+3/2}} \quad (45)$$

The fifth-order limiter is employed, it is proposed by Kim and Kim[2].

$$b_{\mathrm{L}} = \frac{1}{30}\left[-2/r_{\mathrm{L},i-1} + 11 + 24r_{\mathrm{L},i} - 3r_{\mathrm{L},i}r_{\mathrm{L},i+1}\right], \quad (46)$$

$$b_{\mathrm{R}} = \frac{1}{30}\left[-2/r_{\mathrm{R},i+2} + 11 + 24r_{\mathrm{R},i+1} - 3r_{\mathrm{R},i+1}r_{\mathrm{R},i}\right]. \quad (47)$$

Where monotonicity is maintained by limiting the fifth-order extrapolation by using

$$f(r_{\mathrm{L}}) = \max\left[0, \min\left[2, 2r_{\mathrm{L},i}, b_{\mathrm{L}}\right]\right] \quad (48)$$

$$f(r_{\mathrm{R}}) = \max\left[0, \min\left[2, 2r_{\mathrm{R},i+1}, b_{\mathrm{R}}\right]\right] \quad (49)$$

The finite difference 5th-order accuracy WENO scheme suggested by Jiang and Shu[3] is used to evaluate the conservative variables. The WENO scheme for a variable $\mathbf{Q}_{i+\frac{1}{2}}^{\mathrm{L}}$ can be written as:

$$\mathbf{Q}_{i+\frac{1}{2}}^{\mathrm{L}} = w_0 q_0 + w_1 q_1 + w_2 q_2 \quad (50)$$

where

$$q_0 = \frac{1}{3}u_{j-2} - \frac{7}{6}u_{j-1} + \frac{11}{6}u_j \quad (51)$$

$$q_1 = -\frac{1}{6}u_{j-1} + \frac{5}{6}u_j + \frac{1}{3}u_{j+1} \quad (52)$$

$$q_2 = \frac{1}{3}u_j + \frac{5}{6}u_{j+1} - \frac{1}{6}u_{j+2} \quad (53)$$

and

$$w_k = \frac{a_k}{a_0 + \cdots + a_{r-1}} \quad (54)$$

$$a_k = \frac{C_k}{(e + IS_k)^2}, \ k = 0,1,2 \quad (55)$$

$$C_0 = 1/10, \ C_1 = 6/10, \ C_2 = 3/10$$

$$IS_0 = \frac{13}{12}\left(u_{j-2} - 2u_{j-1} + u_j\right)^2 + \frac{1}{4}\left(u_{j-2} - 4u_{j-1} + 3u_j\right)^2 \quad (56)$$

$$IS_1 = \frac{13}{12}\left(u_{j-1} - 2u_j + u_{j+1}\right)^2 + \frac{1}{4}\left(u_{j-1} - u_{j+1}\right)^2 \quad (57)$$

$$IS_2 = \frac{13}{12}\left(u_j - 2u_{j+1} + u_{j+2}\right)^2 + \frac{1}{4}\left(3u_j - 4u_{j+1} + u_{j+2}\right)^2 \quad (58)$$

where, e is introduced to prevent the denominator becoming zero. In their paper, e is taken as 10^{-6}. The $\mathbf{Q}^{R}_{i+\frac{1}{2}}$ is constructed symmetrically as $\mathbf{Q}^{L}_{i+\frac{1}{2}}$ at $i+1/2$.

Time Integration

After spatial discretizations of governing equations, the conservation laws reduce to either a scalar or a system of ordinary differential equations in time, which can be written in the form:

$$\frac{d\mathbf{Q}}{dt} = \mathbf{R}(\mathbf{Q}) \quad (59)$$

In this study, a classical fourth-order Range-Kutta method is employed, which can be written as:

$$\mathbf{Q}_i^0 = \mathbf{Q}_i^n \quad (60)$$

$$\mathbf{Q}_i^1 = \mathbf{Q}_i^0 + \tfrac{1}{2}\Delta t\mathbf{R}(\mathbf{Q}_i^0) \quad (61)$$

$$\mathbf{Q}_i^2 = \mathbf{Q}_i^0 + \tfrac{1}{2}\Delta t\mathbf{R}(\mathbf{Q}_i^1) \quad (62)$$

$$\mathbf{Q}_i^3 = \mathbf{Q}_i^0 + \Delta t\mathbf{R}(\mathbf{Q}_i^2) \quad (63)$$

$$\mathbf{Q}_i^{n+1} = \mathbf{Q}_i^0 + \frac{1}{6}\begin{bmatrix}\Delta t\mathbf{R}(\mathbf{Q}_i^0) + 2\Delta t\mathbf{R}(\mathbf{Q}_i^1) \\ +2\Delta t\mathbf{R}(\mathbf{Q}_i^2) + \Delta t\mathbf{R}(\mathbf{Q}_i^3)\end{bmatrix} \quad (64)$$

Computational Results

Computational Setup

We employed experimental condition to computational initial condition, which was axisymmetric supersonic base flow of Herrin and Dutton[10]. Freestream Mach number and a unit Reynolds Number are 2.46 and 45×10^6 respectively. The base radius of cylinder is 31.75*mm*. Detailed experimental condition marked in Table 1.

Table 1. Experiment condition axisymmetric supersonic base flow[4]

M_∞		2.46
r_∞	kg/m^3	0.7549
p_∞	kPa	31.415
T_∞	K	145
U_∞	$m/\sec$	593.8
Re	m^{-1}	45×10^6

Grid used a cylinder length $8R_0$, where R_0 is base radius. This length was determined by computing flat plate problem with in house code that was included Meter's SST turbulence model. From computing result, boundary layer properties are matched approach boundary properties of Mathur and Dutton[11] experimental data. Boundary layer thickness, displacement thickness, momentum thickness and skin friction were 3.24mm, 0.77mm, 0.22mm and 0.0017 respectively in approach boundary properties of experiment. For skin friction, computational result was 0.00165, it was 2% difference value of experiment data. Other properties of boundary layer are below 10% difference values of experiment datat.

The outflow was $10R_0$ downstream from base. The farfield boundary was $4.15R_0$ from the axis of symmetry. These were the same dimension of Forsythe *et al.* [12] computing grid.

The first y^+ was 4 on the wall and 20 grid points was even spacing within boundary layer. The farfield boundary was clustered grid in Fig. 1. Coarse and middle grids were 0.35×10^6 and 1.52×10^6. The cylinder wall boundary was assigned no slip adiabatic condition. The farfield and outflow boundary were assigned extrapolation.

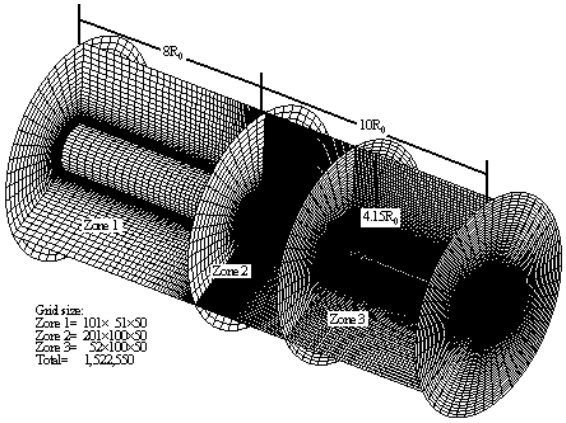

Fig. 1 Base flow grid.

Base flow property

Steady state RANS results of two different turbulence models were agreement with experiment velocity profile within boundary layer at 1mm prior from base in fig. 2. The cylinder length and first y^+ were appropriated from steady state RANS calculation.

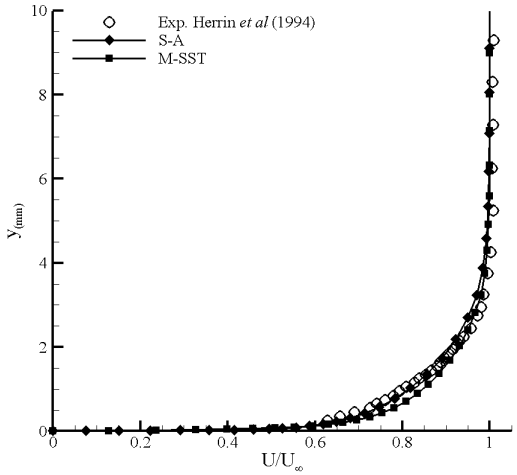

Fig. 2 Boundary Layer profile 1mm prior to the base.

All computing cases of base pressure distribution were similar trend of experimental data in fig. 3. S-A DDES was similar to experimental data, but others were similar to steady state RANS result. These results were not good fit experiment data, because the results supposed low grid resolution on the cylinder base. Our previous 2-dimensional test case had 3 times grid resolution than 3-dimentional test cases on the cylinder base.

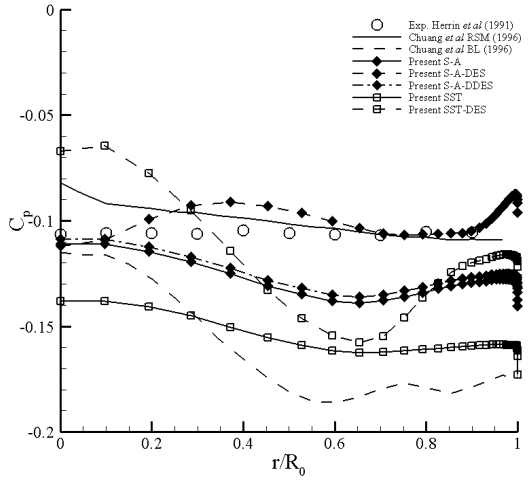

Fig. 3 Base pressure distribution.

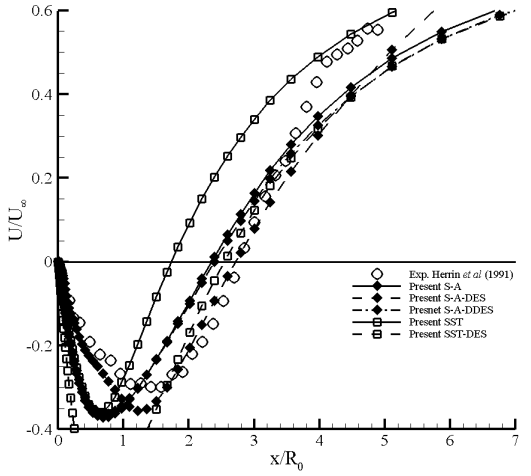

Fig. 4 Velocity profile along center.

Reattachment location of experiment was $x/R_0 \approx 2.8$, but All computing cases were located between $x/R_0 = 2.3 \sim 2.8$ except SST result in fig. 5. S-A DES result showed good to match the reattachment location. The velocity profile in recirculation zone were not matched all computing cases. However, after reattachment location, all velocity profiles were similar trend to experiment.

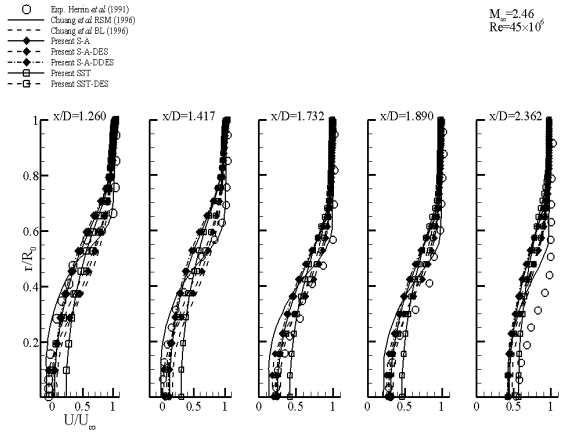

Fig. 5 downstream velocity profile along x-axis.

For downstream velocity profile, velocity profiles of S-A and S-A DES cases were good agreement with experiment data in recirculation zone $x/D \approx 1.26$ in fig. 5.

In reattachment location $x/D \approx 1.417$, S-A DES and SST-DES cases were good agreement with experiment data in fig. 5. However, after reattachment location, all cases were not matched experiment data.

Conclusion

Detached Eddy Simulation is capable to predict in massive separation flow. Strelet DES model was applied present supersonic base flow problem. Supersonic base flow simulations were carried out with DES/DDES of modified Spalart-Allmaras one-equation turbulence model and Menter's SST turbulence model. In base pressure distribution, S-A, S-A DES and S-A DDES showed good results to compare experiment. But S-A DES was slightly over predicted and S-A and S-A DDES were slightly under predicted. In velocity profile along center, most test cases good predicted reattachment location. Better model was S-A DES. In downstream velocity profile after base, S-A DES and SST-DES were good agreement with experiment data nearby reattachment location. But all test cases were not good prediction far distance from reattachment location. The grid of test problem was still not dense near base and reattachment location. Delayed/detached eddy simulation of Spalart-Allmaras model was better feature from these results in supersonic base flow problem. Future works are needed dense grid study, because of good prediction of supersonic base flow features.

Acknowledgments

This work was supported by DAPA (Defense Acquisition Program Administration) through ADD (Agency for Defense Development) of Republic of Korea government.

References

1) Shin, J.-R., Choi, J.-Y. and Kim, C.-G., "CFD Analysis and Validation of Base-Bleed Flow," Proceedings of the 2005 KSAS Spring Conference, pp.504-508, 2005.
2) Kim, K. H. and Kim, C., "Accurate, efficient and monotonic numerical methods for multi-dimensional compressible flows Part II: Multi-dimensional limiting process," *Journal of Computational Physics*, Vol. 208, pp. 570-615, 2005.
3) Jiang, G. S. and Shu, C. W., "Efficient implementation of weighted ENO schemes," *Journal of Computational Physics*, vol. 126, pp. 202-228, 1996.
4) Roe, P. L., " Approximate Riemann Solvers, Parameter Vectors, and Difference

Schemes," *Journal of Computational Physics*, vol. 135, pp. 250- 258, 1997.

5) Wada, Y. and Liou, M.-S., "AN ACCURATE AND ROBUST FLUX SPLITTING SCHEME FOR SHOCK AND CONTACT DISCONTINUITIES," *SIAM J. Sci. Comput.*, vol. 18, No. 3, pp. 633-657, 1997.
6) Strelets, M., " Detached Eddy Simulation of Massively Separated Flows," AIAA Paper No. 2001-0879
7) Spalart, P. R., Deck, S., Shur, M. L., Squires, K. D., Strelets, M. K., and Travin, A., " A new version of detached-eddy simulation, resistant to ambiguous grid densities," *Theor. Comput. Fluid Dyn.*, Vol. 20, pp. 181-195, 2006.
8) Wilcox, D.C., "Turbulence Modeling for CFD," DCW Industries, Inc., 1st edition, 1993.
9) Shur, M., Spalart, P. R., Strelets, M., Travin, A., "Detached-eddy simulation of an airfoil at high angle of attack," proceedings of 4th international symposium on engineering turbulence modeling and measurements, Corsica, Elsevier, pp. 24–26, 1999.
10) Herrin, J. L., and Dutton, J. C., " Supersonic Near Wake Afterbody Boattailing Effects on Axisymmetric Bodies," *J. Spacecr. & Rockets*, Vol. 31, No. 6, pp. 1021-1028, 1994.
11) Mathur, T., and Dutton, J. C., " Base Bleed Experiments with a Cylindrical Afterbody in Supersonic Flow," *J. Spacecr. Rockets*, Vol. 33, No. 1, 1996.
12) Forsythe, J. R., Hoffmann, K. A., Cummings, R. M., and Squires, K. D., " Detached-Eddy Simulation with Compressibility Corrections Applied to a Supersonic Axisymmetric Base Flow," *J. Fluids Eng*. Vol. 124. pp. 911-923. 2002.